

AutoFFS: Adversarial Deformations for Facial Feminization Surgery Planning

Paul Friedrich¹, Florentin Bieder¹, Florian M. Thieringer^{1,2}, and Philippe C. Cattin¹

¹ Department of Biomedical Engineering, University of Basel, Allschwil, Switzerland

² Department of Oral and Cranio-Maxillofacial Surgery, University Hospital Basel, Basel, Switzerland
paul.friedrich@unibas.ch

Abstract. Facial feminization surgery (FFS) is a key component of gender affirmation for transgender and gender diverse patients, aiming to reshape craniofacial structures toward a female morphology. Current surgical planning procedures largely rely on subjective clinical assessment, lacking quantitative and reproducible anatomical guidance. We therefore propose **AutoFFS**, a novel data-driven framework that generates counterfactual skull morphologies through adversarial free-form deformations. Our method performs a *deformation-based targeted adversarial attack* on an ensemble of pre-trained binary sex classifiers that learned sexual dimorphism, effectively transforming individual skull shapes toward the target sex. The generated counterfactual skull morphologies provide a quantitative foundation for preoperative planning in FFS, driving advances in this largely overlooked patient group. We validate our approach through classifier-based evaluation and a human perceptual study, confirming that the generated morphologies exhibit target sex characteristics. Our code is available at <https://github.com/pfriedri/autoffs>.

Keywords: Facial Feminization Surgery · Counterfactual Shape Editing · Adversarial Deformations.

1 Introduction

Gender affirmation surgeries enable transgender and gender diverse patients to align their physical appearance with their gender identity.³ For many transgender women, facial feminization surgery (FFS) represents a critical component of this process. FFS encompasses a wide range of craniomaxillofacial procedures designed to reshape masculine-appearing facial features into more feminine structures [33]. Common procedures include mandibular setback, genioplasty, rhinoplasty, forehead cranioplasty, and fronto-orbital reshaping [2,5]. These surgeries play an essential role in gender transition and have been shown to significantly improve quality of life for transgender women [1,11,14]. Despite these

³ Throughout this paper, we distinguish between *sex* and *gender*. Sex refers to biological and anatomical characteristics (such as skeletal morphology), while gender refers to an individual’s internal sense of identity and social role.

documented benefits, surgeons face considerable challenges in preoperative planning. The literature describes a wide variety of surgical techniques, yet selecting appropriate procedures for each patient’s unique facial anatomy remains difficult [22,33]. Current planning approaches largely rely on experience and subjective assessment, leaving room for data-driven tools that could provide more objective guidance. To close this gap, we propose a novel framework for preoperative planning, called **AutoFFS**, that generates counterfactual skull morphologies, answering the question: *What would this skull look like if it had the opposite sex?* Our approach employs a free-form deformation (FFD)-based *targeted adversarial attack* [8] on an ensemble of pre-trained binary sex classifiers, effectively deforming a given skull toward the desired sex, and supporting personalized surgical planning grounded in anatomical data. While this study focuses on FFS, which accounts for the majority of facial gender-affirming surgeries, the proposed method could also be applied to facial masculinization surgeries (FMS).

Related Work Early work on computer-assisted FFS planning primarily focused on developing virtual surgery planning procedures [15,28,30,31], often involving CAD-based methods for preoperative cutting guide design [16,17]. More recent studies have explored automatic planning and cutting guide generation for isolated anatomical regions, such as the mandible [6] or the lower jaw [25]. Despite these advances, existing methods largely rely on subjective assessment, experience, or reference morphologies [10], and fail to account for the global morphological interdependencies across the entire skull.

Deep learning based methods have demonstrated remarkable capacity to model discriminative sexual dimorphisms, i.e., different morphological characteristics based on a subject’s sex, and have successfully been applied to sex classification tasks [9,12,26]. Building upon this foundation, we propose using these learned representations to generate counterfactual skull morphologies.

2 Method

Problem Formulation Let \mathcal{D} denote a dataset of skull shapes with N samples $\mathcal{D} := \{(\mathbf{X}_i, y_i)\}_{i=1}^N$, where each skull is represented by a function $\mathbf{X}_i : \Omega \rightarrow \mathbb{R}$ mapping spatial coordinates to occupancy values. Here, $\Omega \subset \mathbb{R}^3$ denotes the image domain with discrete dimensions $H \times W \times D$, and $y_i \in \{0, 1\}$ denotes a binary sex label: (0) male, (1) female. We propose to solve FFS planning by finding a conditional deformation field $\Phi_{y_{\text{target}}} : \Omega \rightarrow \Omega$ that maps each spatial coordinate \mathbf{x} to a new coordinate $\Phi_{y_{\text{target}}}(\mathbf{x})$, such that the transformed skull \mathbf{X}' exhibits features of the target sex y_{target} :

$$\mathbf{X}' = \mathbf{X} \circ \Phi_{y_{\text{target}}}. \tag{1}$$

Here, the composition $(\mathbf{X} \circ \Phi_{y_{\text{target}}})(\mathbf{x}) = \mathbf{X}(\Phi_{y_{\text{target}}}(\mathbf{x}))$ defines the deformed image by resampling the original image at the deformed coordinates. In practice, images are discretized on a regular grid, and we use trilinear interpolation

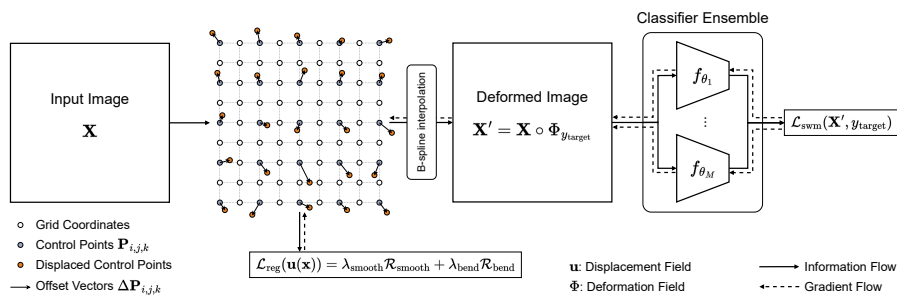


Fig. 1: Overview of the proposed pipeline. We perform a *deformation-based targeted adversarial attack* on an ensemble of pre-trained binary sex classifiers by optimizing the deformation field given the target class label y_{target} . Illustration is in 2D for visualization purposes, but the pipeline works in 3D.

to evaluate \mathbf{X} at non-grid positions during the resampling operation. To find such a deformation field $\Phi_{y_{\text{target}}}$, we propose to perform a *targeted adversarial attack* [8] on an ensemble of pre-trained binary sex classifiers, i.e., we optimize the deformation field such that the transformed scan maximizes the desired class probability. An overview of our proposed approach is shown in Figure 1.

Classifier Training To learn a normative representation of the population in our dataset \mathcal{D} , we train classification networks to solve a binary sex classification task. Through this task, the networks implicitly learn discriminative features that characterize male and female populations. Formally, each classifier is defined as a neural network $f_{\theta} : \Omega \mapsto [0, 1]$ with parameters θ that operates on the discretized image representation. The network parameters are trained using Binary Cross-Entropy (BCE) over a batch of B images from the training set

$$\mathcal{L}_{\text{class}} := -\frac{1}{B} \sum_{i=1}^B \left[y_i \log(f_{\theta}(\mathbf{X}_i)) + (1 - y_i) \log(1 - f_{\theta}(\mathbf{X}_i)) \right]. \quad (2)$$

To enhance the robustness and representation capacity of our proposed approach, we train an ensemble of M classifiers $\{f_{\theta_m}\}_{m=1}^M$ with different architectures. We motivate this choice by the observation that fooling multiple classifiers, each learning distinct feature representations, is substantially more challenging than fooling a single network [21,27]. Consequently, the ensemble approach yields more robust representations that better capture population-level characteristics. Implementation and training details can be found in Section 3.

Free-Form Deformation We parameterize our deformation field Φ as a 3D cubic B-spline FFD [29]. A regular control lattice is defined over the scan domain Ω with $n_x \times n_y \times n_z$ control points $\mathbf{P}_{i,j,k} \in \mathbb{R}^3$. Each control point has

an associated offset $\Delta\mathbf{P}_{i,j,k}$, which defines its displacement from the initial lattice position. The continuous displacement field \mathbf{u} at any spatial location \mathbf{x} is obtained through cubic B-spline interpolation of the control point offsets

$$\mathbf{u}(\mathbf{x}) = \sum_{l=0}^3 \sum_{m=0}^3 \sum_{n=0}^3 B_l(\xi) B_m(\eta) B_n(\zeta) \Delta\mathbf{P}_{i+l,j+m,k+n}, \quad (3)$$

where B denotes a cubic B-spline basis function, (i, j, k) is the index of the cell containing \mathbf{x} , and $(\xi, \eta, \zeta) \in [0, 1]^3$ are the local coordinates within that cell. The resulting deformation field is then defined as

$$\Phi(\mathbf{x}) = \mathbf{x} + \mathbf{u}(\mathbf{x}). \quad (4)$$

Given any differentiable loss \mathcal{L} that depends on the deformed image $\mathbf{X}' = \mathbf{X} \circ \Phi$, the gradient with respect to a control-point offset follows from the chain rule

$$\frac{\partial \mathcal{L}}{\partial \Delta\mathbf{P}_{i,j,k}} = \sum_{\mathbf{x} \in \Omega} B_l(\xi) B_m(\eta) B_n(\zeta) \frac{\partial \mathcal{L}}{\partial \mathbf{X}'(\mathbf{x})} \nabla \mathbf{X}(\Phi(\mathbf{x})), \quad (5)$$

where (l, m, n) are the basis function indices corresponding to control point (i, j, k) within the local $4 \times 4 \times 4$ support region of \mathbf{x} , $\frac{\partial \mathcal{L}}{\partial \mathbf{X}'(\mathbf{x})}$ is the gradient propagated from the loss to the deformed image intensity at location \mathbf{x} , and $\nabla \mathbf{X}(\Phi(\mathbf{x}))$ is the spatial gradient of the original image evaluated at the warped coordinate. This enables end-to-end differentiation of the loss \mathcal{L} with respect to all control-point offsets. We will make use of this property when optimizing our deformation field at test time.

Regularizing the Deformation Field While adversarial optimization can effectively drive the deformation process, it is likely to produce unrealistic, non-smooth transformations if unconstrained. We therefore apply two regularization terms: (1) A *smoothness regularizer*, proposed by Balakrishnan et al. [3], that penalizes the Jacobian of the displacement field

$$\mathcal{R}_{\text{smooth}} = \frac{1}{|\Omega|} \sum_{\mathbf{x} \in \Omega} \left\| \frac{\partial \mathbf{u}(\mathbf{x})}{\partial \mathbf{x}} \right\|_F^2, \quad (6)$$

where $\|\cdot\|_F$ denotes the Frobenius norm, and (2) a *bending energy regularizer* proposed by Rueckert et al. [29] that can be formulated as the discrete, averaged squared Frobenius norm of the Hessian of $\mathbf{u}(\mathbf{x})$

$$\mathcal{R}_{\text{bend}} = \frac{1}{|\Omega|} \sum_{\mathbf{x} \in \Omega} \left(\sum_{p \in \{x,y,z\}} \left\| \frac{\partial^2 \mathbf{u}(\mathbf{x})}{\partial p^2} \right\|_2^2 + 2 \sum_{\substack{p,q \in \{x,y,z\} \\ p < q}} \left\| \frac{\partial^2 \mathbf{u}(\mathbf{x})}{\partial p \partial q} \right\|_2^2 \right). \quad (7)$$

Both regularization terms penalize rapid spatial variations in the displacement field, encouraging smooth, physically plausible transformations. We approximate both terms using finite differences on the deformation grid.

Deformation-Based Targeted Adversarial Attack To apply our method at test time, we perform a *targeted adversarial attack* on the pre-trained classifier ensemble $\{f_{\theta_m}\}_{m=1}^M$ by optimizing our deformation field $\Phi_{y_{\text{target}}}$ to produce a deformed scan \mathbf{X}' that fools these classifiers into predicting the target class label y_{target} . We freeze all classifier weights and only optimize the control point offsets $\Delta\mathbf{P}_{i,j,k}$, which are initialized to zero (identity transform). To optimize these control points, we introduce a *smooth worst-case margin loss* \mathcal{L}_{swm} based on the log-sum-exp operator [7], which smoothly approximates the worst-case logit across the ensemble, targeting the most resistant classifier while maintaining gradient flow through all ensemble members, pushing all classifiers beyond a defined logit-margin γ . The temperature parameter τ controls the smoothness of this approximation, where lower values approach the true min/max. To enforce symmetric deformations, we additionally apply the classifier ensemble to deformed scans mirrored across the midsagittal plane (denoted with $\text{flip}(\cdot)$). The whole process is described in Algorithm 1.

Algorithm 1 Targeted Adversarial Attack at Test Time

Input: Input image \mathbf{X} , target class y_{target} , classifier ensemble $\{f_{\theta_m}\}_{m=1}^M$, iterations S , logit-margin γ , temperature τ , learning rate α , regularization weights $\lambda_{\text{smooth}}, \lambda_{\text{bend}}$
Output: Deformed image \mathbf{X}'

- 1: $\Delta\mathbf{P}_{i,j,k} \leftarrow \mathbf{0}$ ▷ Initialize control point offsets
- 2: **for** $s = 1$ to S **do**
- 3: $\mathbf{u} \leftarrow \text{BSplineInterpolate}(\Delta\mathbf{P})$ ▷ Compute displacement field (Eq. (3))
- 4: $\Phi_{y_{\text{target}}} \leftarrow \mathbf{x} + \mathbf{u}(\mathbf{x})$ ▷ Compute deformation field (Eq. (4))
- 5: $\mathbf{X}' \leftarrow \mathbf{X} \circ \Phi_{y_{\text{target}}}$ ▷ Apply deformation (Eq. (1))
- 6: $\{l_m\}_{m=1}^{2M} \leftarrow \{f_{\theta_m}(\mathbf{X}'), f_{\theta_m}(\text{flip}(\mathbf{X}'))\}_{m=1}^M$ ▷ Obtain ensemble logits
- 7: **if** $y_{\text{target}} = 1$ **then** ▷ FFS - Feminization
- 8: $\tilde{l}_{\min} \leftarrow -\tau \log \sum_{m=1}^{2M} \exp(-l_m/\tau)$ ▷ Smooth minimum
- 9: $\mathcal{L}_{\text{swm}} \leftarrow \max(0, \gamma - \tilde{l}_{\min})$
- 10: **else** ▷ FMS - Masculinization
- 11: $\tilde{l}_{\max} \leftarrow \tau \log \sum_{m=1}^{2M} \exp(l_m/\tau)$ ▷ Smooth maximum
- 12: $\mathcal{L}_{\text{swm}} \leftarrow \max(0, \gamma + \tilde{l}_{\max})$
- 13: **end if**
- 14: $\mathcal{L}_{\text{total}} \leftarrow \mathcal{L}_{\text{swm}} + \lambda_{\text{smooth}}\mathcal{R}_{\text{smooth}} + \lambda_{\text{bend}}\mathcal{R}_{\text{bend}}$ ▷ Aggregate total loss
- 15: Backpropagate $\mathcal{L}_{\text{total}}$ to obtain $\nabla_{\Delta\mathbf{P}}\mathcal{L}_{\text{total}}$ ▷ Eq. (5)
- 16: $\Delta\mathbf{P} \leftarrow \text{Adam}(\Delta\mathbf{P}, \nabla_{\Delta\mathbf{P}}\mathcal{L}_{\text{total}}, \alpha)$ ▷ Update control point offsets
- 17: **end for**
- 18: **return** \mathbf{X}'

3 Experiments

Dataset While most FFS planning approaches rely on computed tomography (CT) imaging, ethical and practical constraints limit access to full-skull CT

scans from healthy individuals. We therefore utilize magnetic resonance (MR) scans of multiple sclerosis patients from the SMSC study [13]. As MS lesions are confined to the brain and spinal cord, the cranial bone morphology remains unaffected, making this dataset a suitable surrogate for studying skull shape variation. The dataset comprises 444 MR scans (152 male, 292 female). Since our analysis targets skull morphology, we preprocessed all scans by first segmenting bone structures using a pre-trained model from GRACE [32]. Each scan was then reoriented to RAS+ convention, padded to $256 \times 256 \times 256$ voxels, and cropped to the frontal half ($256 \times 256 \times 128$) to isolate facial features. The dataset was partitioned into training (70%), validation (15%), and test (15%) sets.

Classifier Training & Performance Our proposed framework relies on accurate sex classification to guide the optimization process. We therefore trained a diverse set of models, including four ResNets [18] ($\text{ResNet}\{18, 34, 50, 101\}$) and four Squeeze-and-Excitation (SE)-ResNets [19] ($\text{SE-ResNet}\{18, 34, 50, 101\}$). All networks were trained with a batch size of 16 for 100 epochs using AdamW [24] with a learning rate of 10^{-4} . To improve generalization, we applied data augmentation during training, including horizontal flipping ($p = 0.5$) and affine transformations ($p = 1.0$) with scaling $s \sim \mathcal{U}(0.9, 1.1)$, rotations $r_x, r_y, r_z \sim \mathcal{U}(-5^\circ, 5^\circ)$, and translations $t_x, t_y, t_z \sim \mathcal{U}(-10, 10)$ voxels. As we require localized features to effectively drive the optimization process, we apply a *masking strategy* during training. We split the volume into $64 \times 64 \times 32$ sized patches and randomly mask 50% in each iteration. To account for class imbalance, we weight the BCE loss by the inverse class frequencies. All models were trained on the same dataset split, with model selection based on validation accuracy. We first evaluate the

Table 1: Classifier performance on the hold-out test set.

Depth	ResNet			SE-ResNet		
	Acc. (\uparrow)	F1 (\uparrow)	AUROC (\uparrow)	Acc. (\uparrow)	F1 (\uparrow)	AUROC (\uparrow)
18	0.924	0.932	0.969	0.894	0.904	0.964
34	0.939	0.946	0.979	0.924	0.932	0.988
50	0.924	0.929	0.976	0.848	0.865	0.949
101	0.864	0.880	0.931	0.818	0.842	0.937

trained classifiers performance on a hold-out test set. We measure accuracy, F1 and AUROC scores and report them in Table 1. Overall, we find strong classification performance across architectures, with most models achieving accuracies above 0.85 and AUROC scores consistently exceeding 0.93.

System Level Performance To evaluate our overall approach, we first divide the classifiers into two groups: (1) classifiers used during optimization ($\text{ResNet}\{18, 34, 50\}$, $\text{SE-ResNet}\{34, 50, 101\}$) and (2) hold-out classifiers for

evaluation (ResNet101, SE-ResNet18). We specifically choose evaluation classifiers with different architectures to ensure our approach fools classifiers with different learned representations. We define a control point lattice with $n_x, n_y, n_z = 32$ control points, and optimize for $S = 100$ steps, using Adam [20] with a learning rate of $\alpha = 5 \times 10^{-3}$ that follows a cosine annealing learning rate schedule [23]. We further set $\lambda_{\text{smooth}}, \lambda_{\text{bend}} = 1 \times 10^8$, $\gamma = 4.5$, and $\tau = 1$.⁴ To ensure changes are limited to facial features, we prohibit deformations in the posterior half of the volume by fixing the control point displacements to zero. To evaluate our

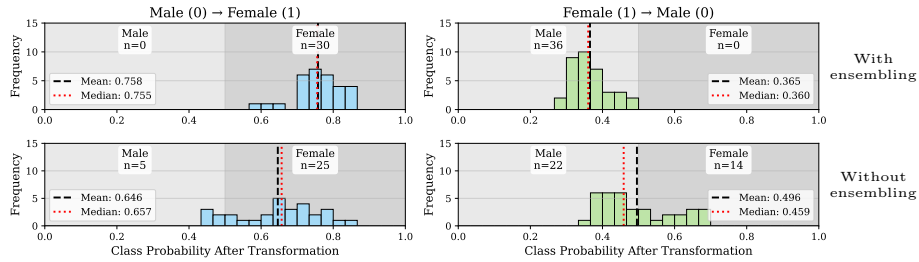


Fig. 2: Class probabilities from the hold-out classifier ensemble after applying our proposed framework with (*top*), and without (*bottom*) the ensembling strategy.

proposed approach, we transform the whole test set and evaluate class probabilities after the deformation process using the hold-out classifiers. As shown in Figure 2 (*top*) our proposed approach consistently generates deformed scans that are classified with the desired sex label, indicating that they exhibit target sex characteristics. We also report scores for our pipeline when using the best classifier (ResNet34) only (*bottom*), highlighting the improved consistency induced by our ensembling strategy. The qualitative examples, shown in Figure 3, demonstrate that the largest deformations appear in regions like the chin, brow ridges, forehead and cheekbones - areas in line with commonly reported sexual dimorphisms [4]. Figure 3 also shows that, without our B-spline formulation and regularization terms, the method collapses to noise-like perturbation patterns, confirming their necessity for constraining the deformations.

Human evaluation We additionally conducted a perceptual study with $N = 11$ participants. Each rater was presented with a total of 80 skulls comprising 20 real male, 20 real female, 20 transformed male (f → m), and 20 transformed female (m → f) samples, displayed in randomized order. Raters were tasked with classifying the original sex of each skull. Five skulls per category were shown two additional times to assess intra-rater agreement. As shown in Table 2, the

⁴ We note that systematic hyperparameter ablation is inherently difficult in our setting, as no ground-truth target morphology or reliable quality metric exists. Hyperparameters were therefore selected based on qualitative assessment.

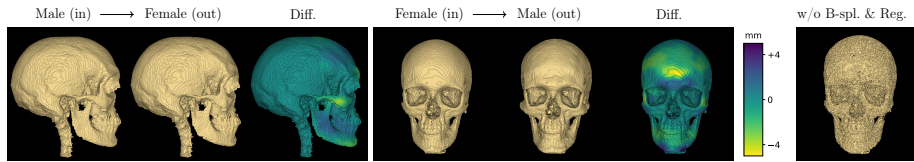


Fig. 3: Example images of a transformed skull. (*Left*) Example FFS from a lateral view. (*Middle*) Example FMS from a frontal view. (*Right*) Example without the B-spline formulation and regularization terms. Best viewed zoomed.

Table 2: Perceptual study results ($N = 11$). We report classification accuracy (mean \pm SD across raters), inter-rater (κ_{inter} , Fleiss’) and intra-rater (κ_{intra} , average pair-wise Cohen’s) agreement.

Category	Acc.	κ_{inter}	κ_{intra}
Real	0.81 ± 0.06	0.51	0.78
Transformed	0.37 ± 0.08	0.37	0.43

raters correctly identified the sex of real skulls with $\sim 81\%$ accuracy (expert anthropologists $\sim 88\%$ [34]), confirming that sexually dimorphic features are perceptible. For transformed skulls, raters perceived the intended target sex in $\sim 63\%$ of cases, significantly above chance, demonstrating that the proposed pipeline produces a systematic perceptual shift ($\Delta_{\text{Acc.}} = 44\%$). This effect was achieved despite the method only modifying anterior facial features while leaving posterior features and overall size unchanged. The lower agreement metrics for transformed skulls suggest that transformed morphologies are perceptually more ambiguous, consistent with the partial modification of sexually dimorphic features.

4 Conclusion

We present **AutoFFS**, a data-driven approach for facial feminization surgery planning that combines learned representations with *deformation-based targeted adversarial attacks*, providing surgeons with objective guidance for facial bone modifications. To successfully generalize our proposed method across diverse skull shapes, ethnicities, and ages, we identify building a large-scale, diverse database as our primary objective for future work. We additionally plan to investigate how the generated morphologies can be integrated into clinical workflows and how, e.g., cutting guides can be derived from them. The presented results suggest that data-driven planning for FFS is a viable research direction with meaningful clinical potential, indicated by both qualitative and quantitative results. We hope this work serves not only as a technical contribution, introducing a novel framework for counterfactual shape editing, but also as an invitation to the community to engage with this largely overlooked problem.

Acknowledgments. We thank Cristina Granziera and Lester Melie-Garcia for providing access to the dataset and Martin Styner for helpful discussions around the evaluation of the method. The Werner Siemens Foundation financially supported this work through the MIRACLE II project.

Disclosure of Interests. The authors have no competing interests to declare that are relevant to the content of this article.

References

1. Ainsworth, T.A., Spiegel, J.H.: Quality of life of individuals with and without facial feminization surgery or gender reassignment surgery. *Quality of Life Research* **19**(7), 1019–1024 (2010)
2. Akhavan, A.A., Sandhu, S., Ndem, I., Ogunleye, A.A.: A review of gender affirmation surgery: What we know, and what we need to know. *Surgery* **170**(1), 336–340 (2021)
3. Balakrishnan, G., Zhao, A., Sabuncu, M.R., Guttag, J., Dalca, A.V.: Voxelmorph: a learning framework for deformable medical image registration. *IEEE transactions on medical imaging* **38**(8), 1788–1800 (2019)
4. Bannister, J.J., et al.: Sex differences in adult facial three-dimensional morphology: application to gender-affirming facial surgery. *Facial Plastic Surgery & Aesthetic Medicine* **24**(S2), S–24 (2022)
5. Becking, A.G., Tuinzing, D.B., Hage, J.J., Gooren, L.J.: Transgender feminization of the facial skeleton. *Clinics in plastic surgery* **34**(3), 557–564 (2007)
6. Beyer, M., et al.: Innovations in gender affirmation: Ai-enhanced surgical guides for mandibular facial feminization surgery. *Clinical Oral Investigations* **29**(8), 1–11 (2025)
7. Boyd, S., Vandenberghe, L.: *Convex Optimization*. Cambridge University Press (2004)
8. Carlini, N., Wagner, D.: Towards evaluating the robustness of neural networks. In: 2017 IEEE Symposium on Security and Privacy (SP). pp. 39–57. Ieee (2017)
9. Çiftçi, R., et al.: Human gender estimation from ct images of skull using deep feature selection and feature fusion. *Scientific Reports* **14**(1), 16879 (2024)
10. Cronin, B.J., Lee, J.C.: Preoperative radiology and virtual surgical planning. *Oral and Maxillofacial Surgery Clinics* **36**(2), 171–182 (2024)
11. Dang, B.N., et al.: Evaluation and treatment of facial feminization surgery: part ii. lips, midface, mandible, chin, and laryngeal prominence. *Archives of Plastic Surgery* **49**(01), 5–11 (2022)
12. Del Bove, A., et al.: Mapping sexual dimorphism signal in the human cranium. *Scientific reports* **13**(1), 16847 (2023)
13. Disanto, G., et al.: The swiss multiple sclerosis cohort-study (smc): a prospective swiss wide investigation of key phases in disease evolution and new treatment options. *PloS one* **11**(3), e0152347 (2016)
14. Dubov, A., Fraenkel, L.: Facial feminization surgery: the ethics of gatekeeping in transgender health. *The American Journal of Bioethics* **18**(12), 3–9 (2018)
15. Escandón, J.M., et al.: Applications of three-dimensional surgical planning in facial feminization surgery: a systematic review. *Journal of Plastic, Reconstructive & Aesthetic Surgery* **75**(7), e1–e14 (2022)

16. Ganry, L., Cömert, M.: Low-cost and simple frontal sinus surgical cutting guide modeling for anterior cranioplasty in facial feminization surgery: how to do it. *Journal of Craniofacial Surgery* **33**(1), e84–e87 (2022)
17. Gutiérrez-Santamaría, J., et al.: Shaping the lower jaw border with customized cutting guides: development, validation, and application in facial gender-affirming surgery. *Facial Plastic Surgery & Aesthetic Medicine* **26**(6), e818–e824 (2024)
18. He, K., Zhang, X., Ren, S., Sun, J.: Deep residual learning for image recognition. In: *Proceedings of the IEEE conference on computer vision and pattern recognition*. pp. 770–778 (2016)
19. Hu, J., Shen, L., Sun, G.: Squeeze-and-excitation networks. In: *Proceedings of the IEEE conference on computer vision and pattern recognition*. pp. 7132–7141 (2018)
20. Kingma, D.P., Ba, J.L.: Adam: A method for stochastic optimization. *arXiv preprint arXiv:1412.6980* (2014)
21. Kurakin, A., et al.: Adversarial attacks and defences competition. In: *The NIPS'17 Competition: Building Intelligent Systems*, pp. 195–231. Springer (2018)
22. Kuruoglu, D., et al.: Point of care virtual surgical planning and 3d printing in facial gender confirmation surgery: a narrative review. *Annals of Translational Medicine* **9**(7), 614 (2021)
23. Loshchilov, I., Hutter, F.: Sgdr: Stochastic gradient descent with warm restarts. *arXiv preprint arXiv:1608.03983* (2016)
24. Loshchilov, I., Hutter, F.: Decoupled weight decay regularization. *arXiv preprint arXiv:1711.05101* (2017)
25. Marin-Montealegre, V., et al.: 3d surgical planning method for lower jaw osteotomies applied to facial feminization surgery. *Annals of 3D Printed Medicine* **15**, 100164 (2024)
26. Noel, L., et al.: Sex classification of 3d skull images using deep neural networks. *Scientific Reports* **14**(1), 13707 (2024)
27. Pang, T., Xu, K., Du, C., Chen, N., Zhu, J.: Improving adversarial robustness via promoting ensemble diversity. In: *International Conference on Machine Learning*. pp. 4970–4979. PMLR (2019)
28. Rancu, A.L., et al.: Virtual surgical planning for facial feminization surgery: Correlation between three-dimensional plans and results varies across procedures. *Plastic and Reconstructive Surgery* pp. 10–1097 (2021)
29. Rueckert, D., et al.: Nonrigid registration using free-form deformations: application to breast mr images. *IEEE Transactions on Medical Imaging* **18**(8), 712–721 (1999)
30. Sanz, D., Ângelo, D.F., Marques, R., Maffia, F., Cardoso, H.J.: F-chin/feminizing the chin: A genioplasty technique with virtual planning for male-to-female transgender patients. *Aesthetic Plastic Surgery* **48**(10), 1899–1905 (2024)
31. Sharaf, B., Kuruoglu, D., Bite, U., Morris, J.M.: Point of care virtual surgical planning and 3d printing in facial feminization surgery. In: *Seminars in Plastic Surgery*. vol. 36, pp. 164–168. Thieme Medical Publishers, Inc. (2022)
32. Stolte, S.E., et al.: Precise and rapid whole-head segmentation from magnetic resonance images of older adults using deep learning. *Imaging Neuroscience* **2**, 1–21 (2024)
33. Tirrell, A.R., El Hawa, A.A.A., Bekeny, J.C., Chang, B.L., Del Corral, G.: Facial feminization surgery: A systematic review of perioperative surgical planning and outcomes. *Plastic and Reconstructive Surgery–Global Open* **10**(3), e4210 (2022)
34. Walker, P.L.: Sexing skulls using discriminant function analysis of visually assessed traits. *American Journal of Physical Anthropology: The Official Publication of the American Association of Physical Anthropologists* **136**(1), 39–50 (2008)